Cytometry
PART A
Journal of the International Society for Advancement of Cytometry

# Detection of Mitochondrial Fission with Orientation-Dependent Optical Fourier Filters

**Robert M. Pasternack, Jing-Yi Zheng, Nada N. Boustany***

Department of Biomedical Engineering, Rutgers University, Piscataway New Jersey 08854

Received 4 May 2010; Revision Received 25 October 2010; Accepted 22 November 2010

Additional Supporting Information may be found in the online version of this article.

Grant sponsor: National Science Foundation; Grant number: DBI-0852857 (to N.B.); Grant sponsor: Rutgers Graduate Presidential Fellowship (to R.P.).

*Correspondence to: Nada N. Boustany, Rutgers University, Biomedical Engineering, Room 320, 599 Taylor Road, Piscatway, NJ 08854, USA

Email: nboustan@rci.rutgers.edu

Published online 3 January 2011 in Wiley Online Library (wileyonlinelibrary.com)

DOI: 10.1002/cyto.a.21011



## Abstract

We utilize a recently developed optical imaging method based on Fourier processing with Gabor-like filters to detect changes in light scattering resulting from alterations in mitochondrial structure in endothelial cells undergoing apoptosis. Imaging based on Gabor filters shows a significant decrease in the orientation of subcellular organelles at 60 to 100 minutes following apoptosis induction and concomitant with mitochondrial fragmentation observed by fluorescence. The optical scatter changes can be detected at low resolution at the whole cell level. At high resolution, we combine fluorescence imaging of the mitochondria with optical Fourier-based imaging to demonstrate that the dynamic decrease in organelle orientation measured by optical Gabor filtering is spatially associated with fluorescent mitochondria and remains largely absent from nonfluorescent subcellular regions. These results provide strong evidence that the optical Gabor responses track mitochondrial fission during apoptosis and can be used to provide label-free, rapid monitoring of this morphological process within single cells. © 2011 International Society for Advancement of Cytometry

## Key terms

mitochondria; light scattering; apoptosis; microscopy

**Mitochondria** have recently emerged at the heart of significant cellular dysfunctions involved in a wide range of diseases, including various myopathies and neurological atrophies, diabetes, cancer, and aging (1), where mitochondrial mutations affect proteins regulating mitochondrial membrane fission/fusion as well as respiratory chain proteins (1,2). In addition, changes in mitochondrial morphology can be induced by mitochondrial functions involved in bioenergetics (3–6). Bcl-2 family proteins, which are the gatekeepers of programmed cell death (apoptosis) regulated by mitochondria, have been shown to influence these bioenergetic processes (7–11). In particular, Bcl-2 proteins may interact with the mitochondrial membrane lipids. For example, truncated Bid (tBid) was shown to bind cardiolipin, which in turn can lead to a change in membrane structure and mitochondrial dysfunction during apoptosis (12). Mitochondria are also more filamentous and interconnected after being exposed to conditions that favor oxidative phosphorylation compared with glycolysis (13). They are more interconnected during the G1-phase of the cell cycle compared with the S-phase (14), and they fragment during apoptosis (15). These findings strongly suggest that the structure and function of mitochondria are linked and that changes in the morphology of mitochondria may act as effectors of important cellular functions.

Several assays have been developed to assess mitochondrial volume changes, such as single angle light scattering methods (90° or forward scatter) including flow cytometry, and absorption spectrophotometry of suspensions of isolated viable mitochondria. These measurements have long been correlated with the morphology of mitochondria in the orthodox and condensed states (16,17), have proved essential in studying the mitochondrial permeability transition (17,18), and have been used to detect volume changes in mitochondria under different conditions including

ISAC
International Society for Advancement of Cytometry

apoptotic cells (19–21). Light scattering spectroscopy and flow cytometry were also used to probe mitochondrial dynamics within living cells (22–25) and tissues (26). However, there are currently no standard assays that are specifically designed to quantify mitochondrial fission in an efficient rapid throughput setting. The morphology of mitochondria can be assessed by electron microscopy (27) or by high-resolution fluorescence microscopy to allow observation, segmentation, and measurement of individual organelles within living cells (28–31). These techniques have low throughput and can be experimentally demanding or costly to implement on a routine basis. Moreover the use of fluorescence labels can interfere with biological function.

Thus, one of the long-term aims underlying the results presented in this study is to investigate the feasibility of developing a rapid light-scattering-based cell assay to quantify subcellular morphological changes associated with mitochondrial fission. In this article, we present a proof-of-concept for detecting mitochondrial fission using an optical Fourier filtering modality based on Gabor filters that we developed recently and that is sensitive to size (32) and orientation (33,34) of sub-micron and micron-sized structures. The method is implemented by analyzing the output of a conventional microscope with a spatial light modulator to infer the scattering properties of the sample object (see also Supp. Info.). To demonstrate the ability of this optical scatter method to detect mitochondrial fission, we utilize a well-known and reproducible model of mitochondrial fission consisting of mitochondrial fragmentation during apoptosis where elongated filamentous mitochondria fragment into shorter and rounder ones in cells treated with staurosporine (STS) (35). Our results suggest that the optical Gabor filtering modality remains sensitive to mitochondrial fragmentation at low image resolution and thus could be applicable to label-free, rapid screening of mitochondrial fission in large fields of living cells. Such an assay could be used in the future as a method to detect fission under different physiological and pathological conditions, and will ultimately help identify the potential bioenergetic factors involved in this process.

## Materials and Methods

### Cell Culture

Bovine Aortic Endothelial Cells (BAEC, Clonetics Lonza, Chicago, IL) are cultured as previously described (36) in 0.22 $\mu$m-filtered low-glucose Dulbecco's Modified Eagle Medium (Invitrogen, Carlsbad, CA) supplemented with 10% FBS (Invitrogen), 1% L-Glutamine (100×) (Invitrogen), 9 mg/mL bovine brain extract (Lonza), 10,000 U/mL Heparin (Sigma Chemical, St Louis, MI), and 1% penicillin/streptomycin (Invitrogen). For fluorescence imaging, the cells are incubated with growth medium supplemented with 100 nM Mitotracker green (Invitrogen) for the last 45 minutes of incubation before viewing. For optical viewing, the cells are grown to ~50% confluence on no. 1 glass coverslips (Fisher Scientific, Pittsburgh PA). The coverslips are mounted as previously described (36) and viewed in $CO_2$-independent Leibovitz L-15 medium (Invitrogen) supplemented with 10% FBS at room temperature and room air. Apoptosis was induced by exchanging the cells' normal viewing medium for viewing medium containing 1 $\mu$M staurosporine (Sigma Chemical) prepared from a 4mM staurosporine stock solution in DMSO (Sigma). Control studies consisted of loading L-15 + 10% FBS with DMSO only in the same volume in place of the STS solution.

### Apoptosis Assay

BAEC are grown on coverslips as described above and then treated under experimental conditions with STS or DMSO for 3 hours. The coverslips are then rinsed with PBS 3x, fixed with 4% paraformaldehyde in PBS at room temperature for 15 minutes. Then, after 3× rinsing with PBS, the cells are permeabilized with 0.1% Triton-100 + 0.1% sodium citrate in PBS at room temperature for 5 minutes and then blocked with 2% FBS in PBS for 60 minutes at 37°C. Cells are then incubated overnight at 4 °C with a fluorescently conjugated antibody to cleaved Caspase-3 (Asp175) (Alexa Fluor 488 Conjugate, #9669, Cell Signaling Technology, Danvers, MA) diluted at 10 $\mu$g/mL (1:100 dilution) in blocking solution and mounted on microscope slides sealed with nail polish for imaging.

### Optical Imaging and Fourier Filtering

All samples are studied on the optical Fourier processing microscope described in (33) fitted and aligned with a 63× oil immersion objective with numerical aperture (NA) = 1.4, or a 20× dry objective with NA = 0.75 (Carl Zeiss, Gottingen, Germany). For Fourier filtering, light from a ~5 mW Helium-Neon laser ($\lambda_o$= 632.8 nm) was passed through a spinning diffuser and coupled into a multimode fiber whose output was collimated and launched into the microscope's condenser aligned in central Köhler illumination (NA < 0.05) to provide a spatially coherent plane wave illumination of the sample. Optically filtered images were acquired on a Cascade 512B charge-coupled device (CCD) (Roper Scientific, Trenton, NJ). Fourier filtering was achieved with a TI0.7XGADMD 1100 Digital Mirror Device (DMD) (Texas Instruments, Dallas, TX) placed in a conjugate Fourier plane outside the microscope side port (Fig. 1). Using the diffraction pattern of a graticule with known line spacing, the position of each mirror in the plane of the DMD is calibrated against spatial frequency. This calibration is performed for each of the two objectives utilized in this study (the 63× oil immersion and the 20× dry objective). Spatial frequency in cycles/$\mu$m is taken as $n \times (\sin\theta)/\lambda_o$. $\theta$ is the diffraction angle incident on the objective, and $n$ is the refractive index of the medium in front of the objective.

Gabor filtering is implemented on the DMD as described in (33). An orientation-sensitive filter bank is used, consisting of Gabor-like filters with orientations $\varphi = 0^\circ$ to $\varphi = 180^\circ$ in $20^\circ$ increments (Fig. 1, inset 1, see also the Supp. Info.). In the object space, the filters have a period $S = 0.9$ $\mu$m and a Gaussian envelope standard deviation $\sigma = S/2 = 0.45$ $\mu$m. In the present study, this period, $S$, corresponds to a spatial frequency, $1/S$, positioned on mirror 91 on the DMD when using the 60× objective, and mirror 141 when using the 20× objective.

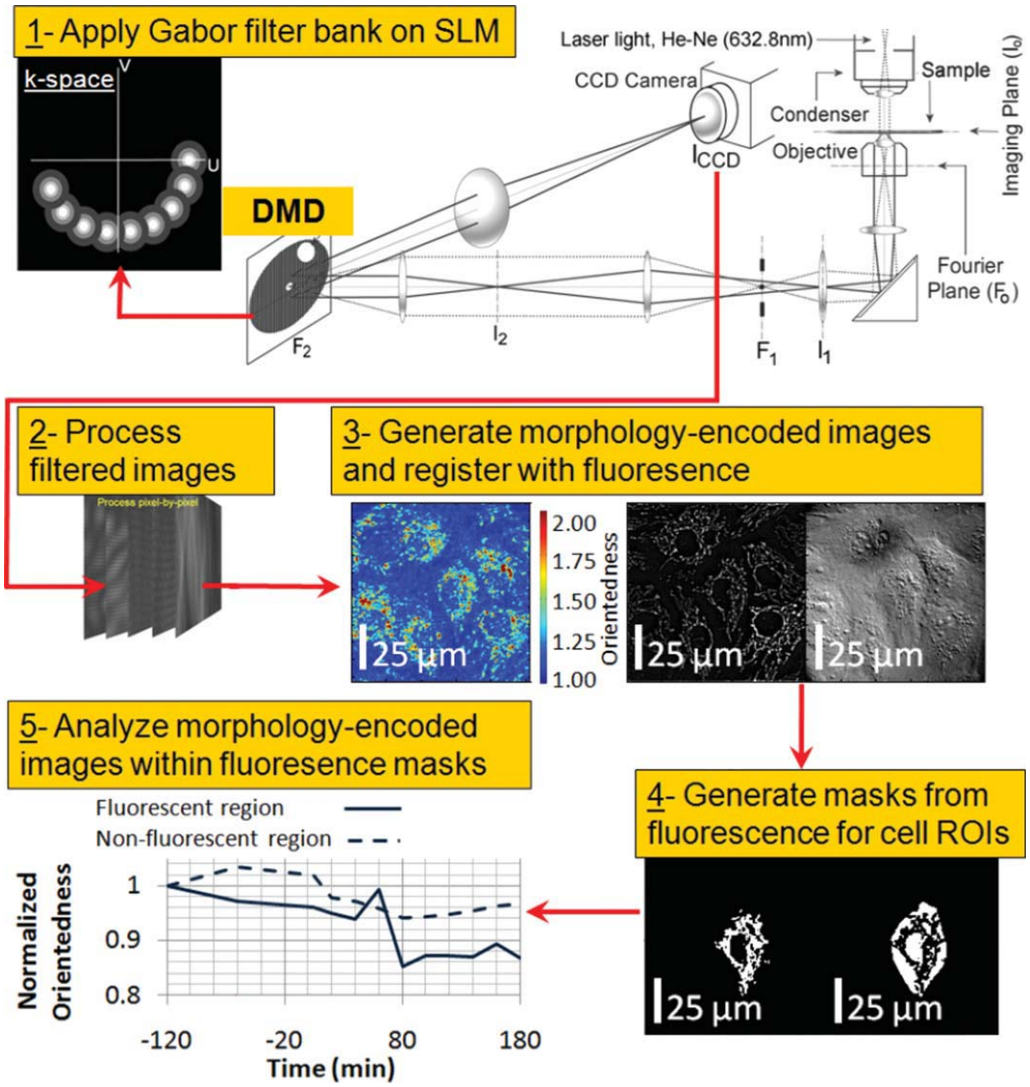


**Figure 1.** Optical setup and data processing. The light scattered by the sample is Fourier-filtered by the DMD (inset 1). The stack of filtered images (inset 2) collected on the CCD is processed pixel-by-pixel and results in morphometrically encoded images (color-coded image) of the object that can be registered directly with the fluorescence and DIC images (inset 3). Masks segregating bright fluorescent regions from dim ones for each cell ROI at each time point (inset 4) allow study of orientation dynamics within regions dominated by mitochondria and those dominated by nonfluorescent subcellular structures (inset 5). [Color figure can be viewed in the online issue, which is available at wileyonlinelibrary.com.]

Fluorescent imaging of the mitotracker-labeled cells is accomplished with a FITC filter cube (filter No. 10; Carl Zeiss, Gottingen, Germany) with 450 to 490 nm excitation bandpass, and emission collected through a 510-nm dichroic mirror followed by a 515 to 565 nm bandpass filter. Fluorescent image acquisition is accomplished without Fourier spatial filtering, bypassing the DMD by sending the light through the trinocular port of the microscope to a CoolSnap CCD (Roper Scientific, Trenton, NJ). Differential interference contrast (DIC) images were also acquired on both the Cascade and the CoolSnap CCDs to aid in image registration. DIC imaging on the Cascade utilized the low NA laser illumination at 0.633 $\mu$m used for optical Fourier filtering; for DIC imaging on the CoolSnap a higher illumination NA was used by briefly bypassing the 0.633 $\mu$m incident laser light by mounting a collimated blue 470 nm LED (Thorlabs, Newton, NJ) to the microscope's condenser arm and opening the condenser aperture.

For dynamic study of apoptosis, the Gabor filter bank is applied in time intervals of 20 minutes over a 3-hour time after STS addition, with each filtered image collected at 6,000 ms exposure. Before STS treatment, and for the cells treated only with DMSO (controls) the optical data were acquired every 50 to 60 minutes. At each timepoint, unfiltered dark field and DIC images are collected immediately before each stack of Gabor filtered images on the Cascade CCD. DIC and fluorescent images are taken on the CoolSnap CCD immediately after collection of the filtered image stack. Gabor-filtered background images consisting of imaging an empty glass sample are collected with

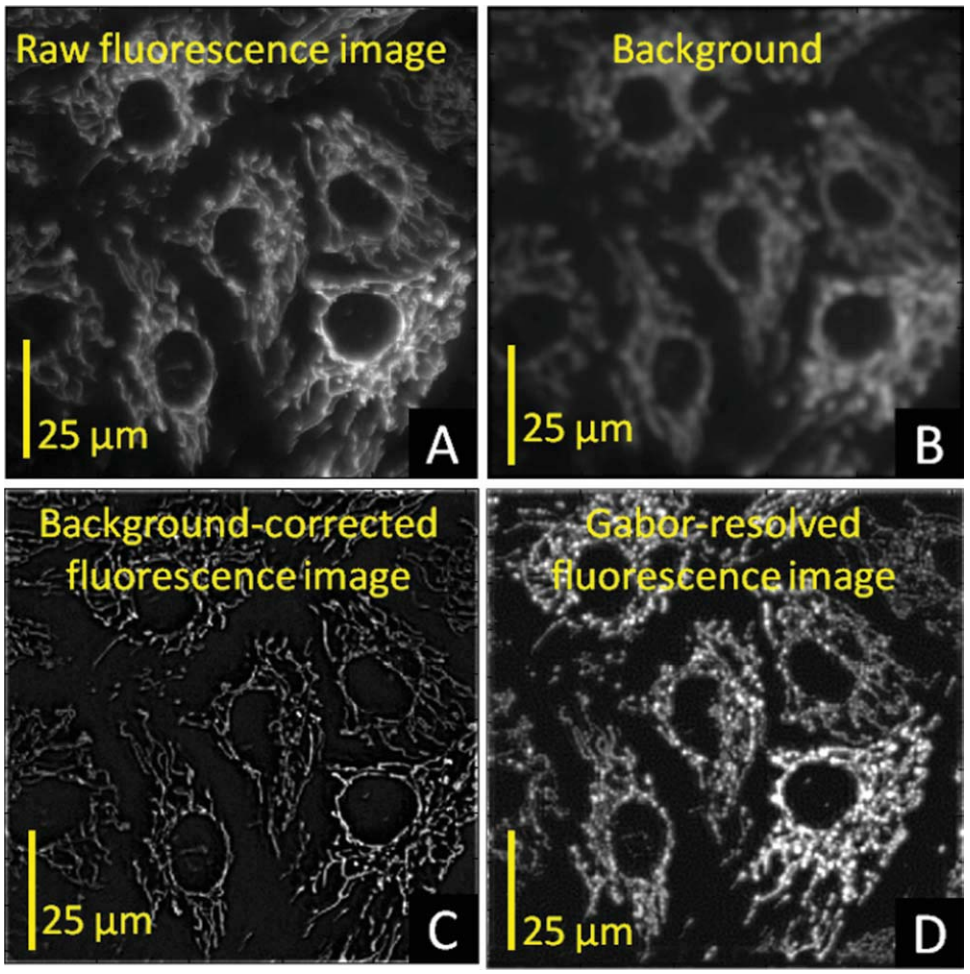


**Figure 2.** Fluorescence image processing. The raw fluorescence image (**A**) is filtered with a lowpass filter. This generates a background image (**B**) which is then subtracted from the original image to generate a high-contrast mitochondrial fluorescence image (**C**). A digital Gabor filterbank with the same orientations, period and Gaussian envelope as the DMD Gabor filters used in the optical setup is applied to the background-corrected fluorescence image to yield a fluorescence image with the same spatial resolution as the optically filtered images (**D**). [Color figure can be viewed in the online issue, which is available at wileyonlinelibrary.com.]

6,000 ms exposure at the start of each experiment at every filter angle $\varphi$, and subtracted from the corresponding filtered images collected during dynamic studies.

### Data Analysis

The background-subtracted Gabor-filtered images are registered with the DIC and fluorescence images. For each time point, the degree of particle orientation, defined as "orientedness," is extracted at each pixel from the Gabor-filtered images by taking the ratio of maximum to average signal response as a function of Gabor filter orientation, $\varphi$, as described in (33), thereby generating "orientedness" response maps of the object (Fig. 1, insets 2 and 3).

At each timepoint, each cell in the field of view is segmented manually into a region of interest (ROI). For whole cell studies, we track the mean orientedness within each ROI (and thus each cell) by plotting the average pixel value within the ROI over time. The mean orientedness per cell is then averaged over all cells studied to yield an average plot of orientedness as a function of time after STS or DMSO treatment. For subcellular analysis, fluorescence labeling of the mitochondria is used to determine the location of mitochondria within the cells studied at high resolution (using the 63× objective). Unsharp masking of the raw fluorescence images is achieved by applying a Gaussian lowpass filter with standard deviation 2 $\mu$m to the raw image and subtracting this image from the raw image (Figs. 2A and 2B). This generates a high-contrast background-corrected fluorescence image highlighting the fluorescently labeled mitochondria (Fig. 2C). The background-corrected fluorescence image is convolved with a digital Gabor filterbank consisting of filters with the same orientation, period and Gaussian envelope as the Gabor filters implemented optically on the DMD ($\varphi$ = 0–180° in 20° increments, $S$ = 0.9 $\mu$m, $\sigma$ = 0.45 $\mu$m). These digitally filtered fluorescence images are then averaged resulting in a Gabor-resolved fluorescence image (Fig. 2D) with the same spatial resolution as the optically filtered data.

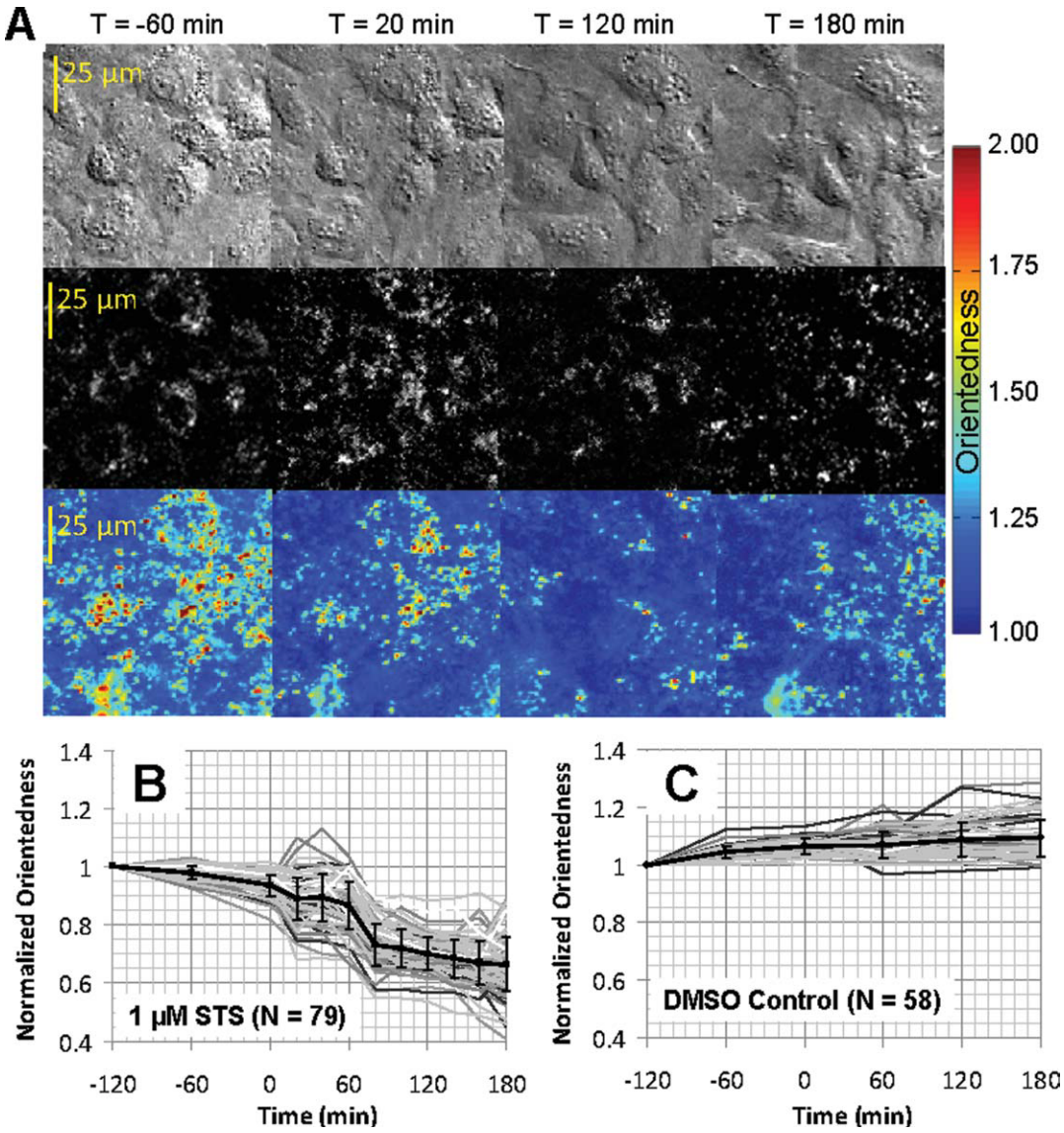


**Figure 3.** Orientedness derived from Gabor-like filter responses for BAEC studied at low resolution (objective NA = 0.75, 0.625 $\mu$m/pixel). (**A**) Images of BAEC exposed to STS taken −60, 20, 120, and 180 minutes from STS exposure ($T = 0$). Top: DIC. Middle, fluorescence images of labeled mitochondria. Little difference in mitochondrial morphology is discernible at these time points at low resolution. Despite this, the morphometric images encoding orientedness (colorscale in bottom panels) report a decrease in orientedness as a function of time after STS addition. (**B** and **C**) Time traces plotting the mean orientedness within individual cells treated with STS (gray traces in B) or DMSO (gray traces in C). In (B) and (C), the solid bold black trace represents the mean ± standard deviation of the individual gray traces. The data were normalized to $T = -120$ minutes.

The processed fluorescence signal within each cell ROI is intensity-thresholded using the mean of the ROI fluorescence intensity as the threshold level. This process is repeated at each timepoint for each field of cells studied. The choice of threshold is discussed in the Results section. Within each cell ROI, this thresholding procedure generates two sets of subcellular regions, one dominated by bright fluorescent mitochondria and the other by the remaining dim background (Fig. 1, inset 4). All pixels within each single cell ROI are included in this analysis. The bright and dim fluorescent areas are then separately applied as a mask to the orientedness encoded Fourier processed images to compare the changes in particle orientedness within the areas rich in mitochondria versus regions dominated by nonfluorescent subcellular structures (Fig. 1, inset 5).

## Results

### Detection of Subcellular Dynamics at Low Magnification

We first acquire images at low resolution using the 20× objective (NA = 0.75, 0.625 $\mu$m/pixel) to investigate if we can detect changes in light scattering at the whole cell level in a relatively large field of view. At each time point, we apply the Gabor filterbank to the whole field of view. As described in

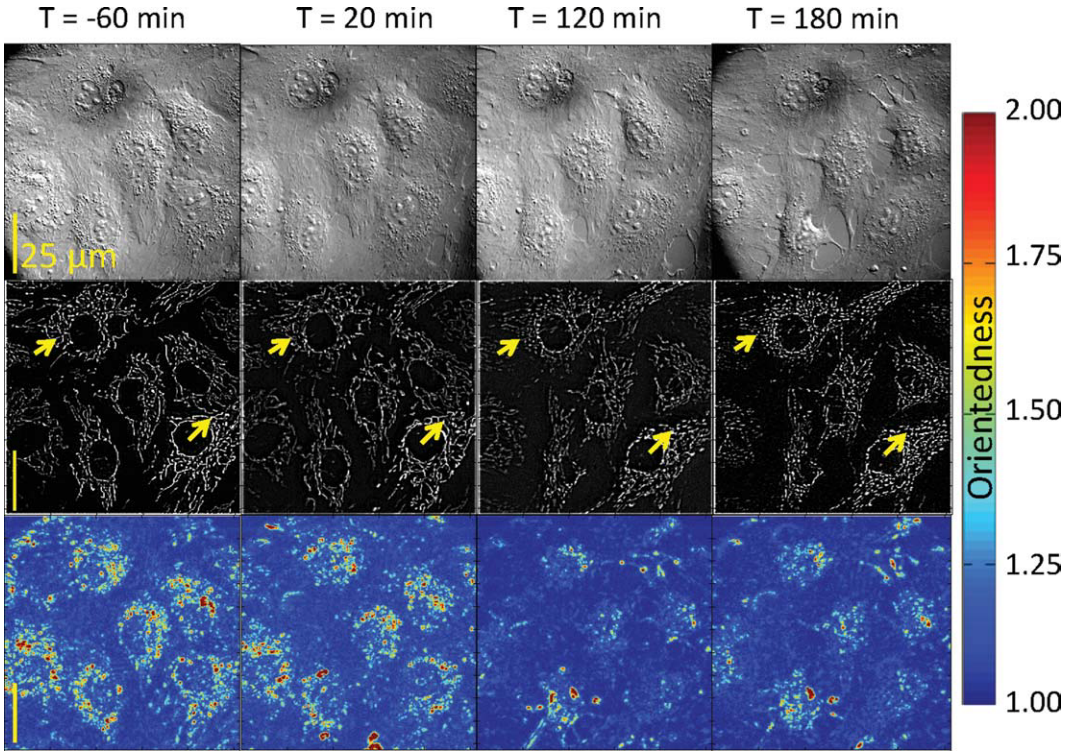


**Figure 4.** High-resolution study of BAEC exposed to STS (objective NA = 1.4, 0.195 $\mu$m/pixel). (**A**) Images of BAEC exposed to STS at −60, 20, 120, and 180 minutes from STS exposure ($T = 0$). Top: DIC. Middle, background-corrected fluorescence images of labeled mitochondria. Arrows point to fragmenting mitochondria. Bottom, morphometric images encoding orientedness (colorscale) reporting decrease in orientedness as a function of time after STS addition at $T = 0$.

Methods, we generate morphometric images encoding orientedness (Fig. 3), which corresponds to the amount of particle orientation at each pixel. The resolution of the corresponding fluorescence images is inadequate to discern any changes in mitochondrial morphology. However, the orientedness data derived from the optical scatter measurements using the Gabor-like filters show that orientedness markedly decreases between 20 and 120 minutes after STS was added as compared with control (Figs. 3B and 3C), indicating a drop in object aspect ratio despite the poor image resolution.

### Validation at High Resolution

To investigate the source of the morphological changes detected by optical Fourier filtering at low resolution, we repeat the studies at high image resolution with the 63× NA = 1.4 objective (sampling at 0.195 $\mu$m/pixel). At high resolution in the fluorescent images, mitochondria evolve from a long, filamentous morphology to shorter, smaller and rounder shapes between 60 and 120 minutes (Fig. 4 see arrows in middle panels). During this time, orientedness (Fig. 4, bottom panels) decreases in the morphometric images. We observe a similar dynamic behavior in orientedness as found at low resolution (Fig. 5).

The resolution gained in the fluorescence image allows for breaking down each cell ROI into two subcellular regions—bright, mitochondria-rich areas in the fluorescence images and dim, mitochondria-poor ones—by applying the thresholding method discussed in the Methods to each cell ROI at each time point. We exploit the high resolution condition to implement this segregation in order to investigate whether the dynamics observed in the cells exposed to STS are spatially associated with the mitochondria. We first studied the segregation of the mitochondria-rich and mitochondria-poor compartments derived for each ROI by modulating the threshold value (Fig. 6). As shown in Figure 6 for a representative cell, when the threshold is set too high, pixels that are clearly fluorescent are designated as nonfluorescent and the optical signal changes in both the fluorescent (above threshold) and nonfluorescent (below threshold) regions (Figs. 6E and 6F). As the threshold is decreased, less of the fluorescent pixels are included in the region designated as non-fluorescent, and the decrease in orientedness becomes more pronounced in the fluorescent segment compared with the nonfluorescent one (Figs. 6B and 6C). For very low thresholds, pixels that are clearly nonfluorescent are designated as fluorescent and the optical signal changes in the fluorescent segment become less pronounced than at higher thresholds (Fig. 6A). By choosing the threshold as the average fluorescence intensity of the cell ROI (and assigning this derived average a value of unity, i.e. Th = 1.0, Fig. 6C), we found that we could arrive at good signal separation between the background and fluorescent areas within the ROI taken at high resolution. We therefore chose this threshold, Th = 1, to derive the fluorescent and non-fluorescent regions in all cells for all time points.

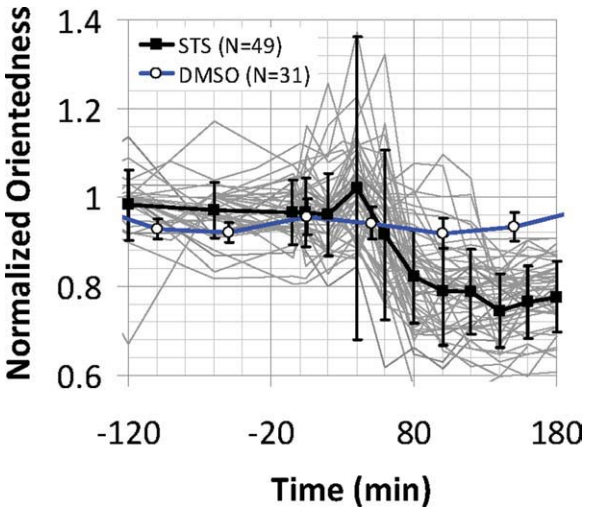


**Figure 5.** Time traces plotting the mean orientedness within individual cells tested at high resolution (objective NA= 1.4, 0.195 $\mu$m/pixel) and treated with STS (gray traces). Bold black trace with solid squares represents the mean ± standard deviation of the gray traces of cells exposed to STS. The blue trace with open circles corresponds to the average orientedness per cell ± standard deviation as a function of time for DMSO control. The STS data were normalized to $T = -180$ minutes; the DMSO data to $T = -200$ minutes. [Color figure can be viewed in the online issue, which is available at wileyonlinelibrary.com.]

Figure 7 shows the results of studying the fluorescent (Fig. 7A) and nonfluorescent regions (Fig. 7B) separately within each cell. In the fluorescent regions, orientedness decreases significantly (Fig. 7A, bold black time trace with solid squares), especially between 60 and 100 minutes ($P < 0.05$ comparing these two timepoints), but does not decrease significantly in the nonfluorescent regions (Fig. 7B, bold black time trace with solid squares). This behavior is different from DMSO control studies (blue traces with open circles in Figs. 7A and 7B), in which neither the fluorescent nor the nonfluorescent regions show such a decrease in orientedness over this timeframe. Thus the optical scattering changes measured by Gabor filtering are isolated to the mitochondria-rich compartment of BAEC during exposure to STS.

We also tracked the relative number of noncontiguous regions within the masks generated for Th = 1. At high resolution, we found that the number of regions within the masks increases by about a factor of 2.5 between 0 and 180 minutes after STS exposure, most of which occurs between 60 and 120 minutes, consistent with mitochondrial fragmentation during this time (Fig. 7C). This behavior is absent when the control data are processed in this manner, suggesting this behavior is STS-specific. When repeating the segmentation process on the low-resolution fluorescence images (Fig. 7D), the masks fail to recapitulate this response; the number of fluorescent segments does not appreciably increase over time or over control, implying that high resolution is required for the masks to be effective in segmenting the mitochondria well.

### Assessment of Movement

To assess movement of the mitochondria between time points as apoptosis and mitochondrial fragmentation proceed, we compared the fluorescent and nonfluorescent masks (using the threshold value Th = 1) at the beginning and end of the entire time span. We find that ~26% of the pixels within a given cell ROI may move from one segment to the other during fragmentation. This necessitated taking new fluorescent images of the cells and defining the fluorescent and non fluorescent regions above and below threshold at every time point. However, movement may also exist in the 7 to 8 minutes time span over which the data set for a single time point is acquired under relatively steady-state conditions, well before or well after fragmentation. Figure 8 shows the prevalence of movement in a 10-min time span after STS addition but well before fragmentation occurs. We acquired fluorescence images over 10 minutes at 5-second intervals for the first minute and then every 15 seconds thereafter. We repeated the process of segmenting each cell ROI into designated fluorescent and nonfluorescent segments above and below the ROI's average fluorescence intensity (Th = 1) and compared these segments at each time point with the initial segments at $T = 0$ in order to quantify movement over the 10 minutes time span. As shown in Figure 8, in the first 15 seconds, only 3% of pixels change between being classified as fluorescent and nonfluorescent. By 1 minute this value rises to 5% and by 10 minutes, 8% of the total number of pixels within the first ROI has changed designation. This effect is most prominent in the periphery of the cell where mitochondrial density is lowest (yellow areas in Fig. 8C). These results suggest that the fluorescent masks remain accurate to within 8% during image acquisition for timepoints away from the moment of fragmentation under approximately steady-state experimental conditions.

### Confirmation of Apoptosis

To confirm the apoptotic fate of the BAEC treated with STS, we assessed the cleavage and activation of caspase 3 by immunofluorescence (Fig. 9). A long exposure (>2 seconds) was used in collecting the fluorescent images. Low intensity background fluorescence is detected within most cells for both treated and control cells. Cells positive for caspase 3 activation are identified as cells with bright fluorescence with intensity at least 50% higher than background levels. After 3 hours of treatment with STS at room temperature, the results show caspase 3 activation in 7.3% of the STS treated cells compared with 0.5% in the cells treated with only DMSO (control). This difference is significant ($P < 0.01$) and provides evidence of apoptosis initiation in the STS-treated cells.

## Discussion

Using optical imaging with Gabor-like filtering, we demonstrate sensitivity to changes in light scattering from BAEC cells undergoing apoptosis in response to STS treatment. We observed a significant drop in the degree of orientation ("orientedness" parameter) of subcellular structures 60 to 100 minutes after apoptosis induction by STS. These scattering changes, which result from alterations in subcellular structure, could be detected and monitored at a low resolution at which subcellular structural dynamics could not be directly visualized by fluorescence or DIC (Fig. 3). These results were

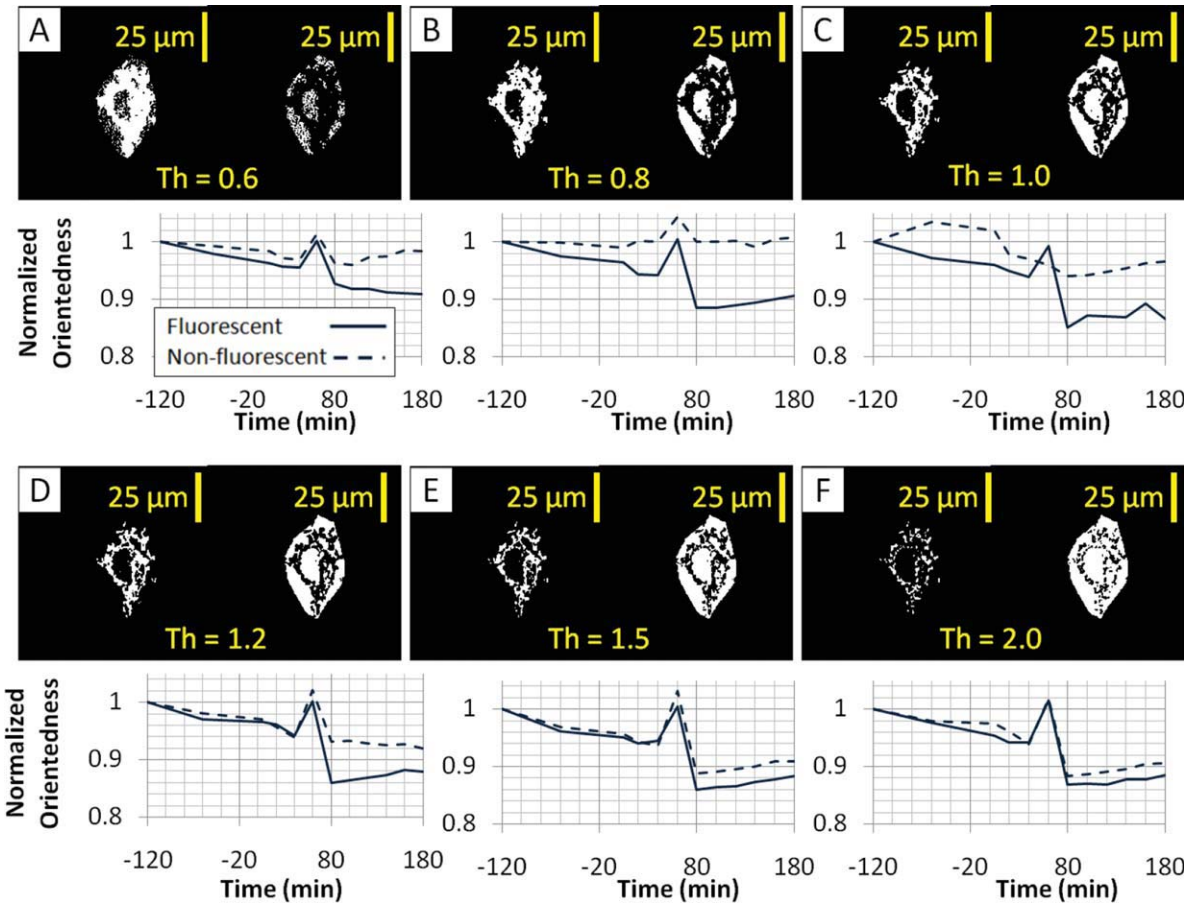


**Figure 6.** Effect of threshold level on separating dynamics of fluorescent and non-fluorescent regions within cell ROIs at high resolution (objective NA= 1.4, 0.195 $\mu$m/pixel). A representative cell from the center of the field of view shown in Figure 4 is illustrated here. (**A**)—(**F**) Show the ''fluorescent'' (above threshold, left) and ''non-fluorescent'' (below threshold, right) region pairs generated by applying a threshold to the corresponding Gabor-resolved fluorescence image (Fig. 2D). The time traces for normalized mean orientedness evaluated within the designated fluorescent mask (above threshold, solid black line) and the nonfluorescent mask (below threshold, dashed line) are shown below the corresponding binary mask images. The threshold level, Th, is given as a fraction of the average fluorescence signal within the cell ROI (e.g. Th = 2.0 indicates that twice the average of the intensity of the Gabor-resolved fluorescence images within that ROI was used to generate the region pair). [Color figure can be viewed in the online issue, which is available at wileyonlinelibrary.com.]

reproduced at high image resolution where they occurred concurrently with mitochondrial fragmentation observed by fluorescence (Figs. 4 and 5). At high resolution, the optical light scatter changes could be isolated to the subcellular compartments dominated by fluorescent mitochondria, while optical scatter changes remained negligible in regions with dim fluorescence signal dominated by nonfluorescent background (nonmitochondria) (Figs. 7A and 7B). Thus, our results strongly suggest that the drop in orientedness between 60 and 100 minutes is due to mitochondrial fragmentation, a process in which relatively large, filamentous structures (contributing to high orientedness) become smaller and rounder (yielding low orientedness).

Validation of the optical scatter signatures is dependent on the ability to label the mitochondria and use this labeling to segment the subcellular mitochondria-rich regions from the remainder of the cell based on a fluorescence intensity threshold as described in Figure 6. Mitochondrial movement is an inherent limitation to the ability of this method. However we find that the two fluorescent segments above and below threshold do not shift by more than 26% over the course of fragmentation and change only by 8% during a 10-minute timespan taken under quasi steady-state conditions. Thus, while mitochondria move during fragmentation, the fluorescent pixels associated with them at a given measurement timepoint remain sufficiently spatially confined within the resolution of the designated fluorescent segment such that we still can separate the background from the dynamic signal associated with mitochondria reasonably well. Our data does not completely exclude the presence of mitochondrial pixels from the background segments below threshold or the presence of some background pixels in the fluorescent segments above threshold. However our data demonstrate that the optical scatter dynamics are significantly reduced, if not completely absent, in cell segments dominated by nonfluorescent organelles (“background”). This suggests that any background con-

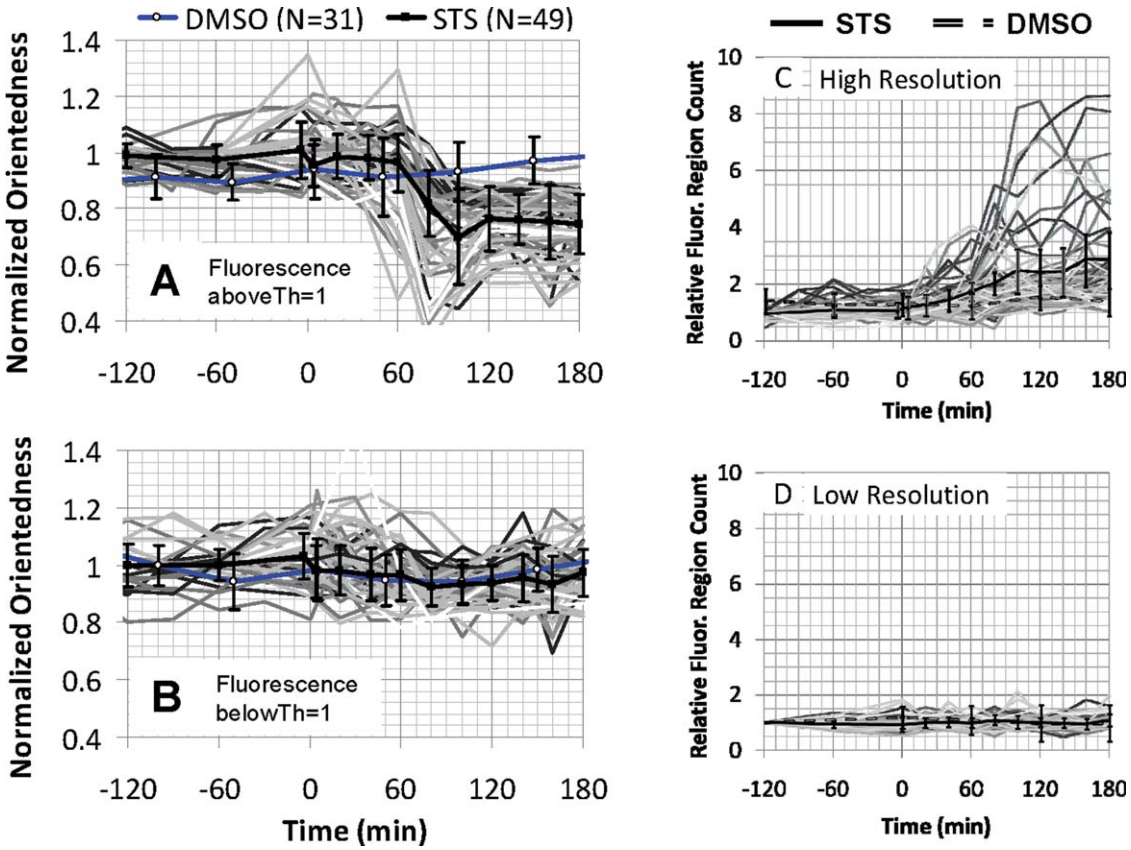


**Figure 7.** (**A**) and (**B**) Time traces plotting orientedness for the bright, above-threshold fluorescent regions (A) and for the dim, below-threshold regions (B) within individual STS-treated cells (gray traces). The average fluorescence intensity in the processed fluorescence image defined the threshold value within each cell and corresponds to Th = 1 (see also Fig. 6). Bold black trace with solid squares represents the mean ± standard deviation of the gray traces of cells exposed to STS. Blue trace with open circles corresponds to the mean ± standard deviation for DMSO control (average of all cells). (**C**) and (**D**) Normalized number of non-contiguous fluorescent regions counted in the above-threshold fluorescent mask generated at high resolution [(C), NA = 1.4, 0.195 $\mu$m/pixel] and at low resolution [(D), NA = 0.75, 0.625 $\mu$m/pixel] with Th = 1. The rise in the number of fluorescent regions beyond $T = 60$ minutes is statistically significant ($P < 0.05$) comparing average STS response with DMSO control at high resolution (C) but is not statistically significant ($P = 0.72$) at low resolution (D). In (C) and (D), bold black trace represents the mean ± standard deviation of the gray traces of cells exposed to STS. Dashed trace corresponds to the mean ± standard deviation for DMSO control (average of all cells). [Color figure can be viewed in the online issue, which is available at wileyonlinelibrary.com.]

tribution to the dynamic scattering signal is likely to be negligible within the brightly labeled regions dominated by the presence of mitochondria. Based on previous work demonstrating the larger contribution of mitochondria to the light scatter signal relative to other organelles (36–38), we may also assume that other organelles present in close association with the mitochondria (e.g. the endoplasmic reticulum) do not contribute appreciably to the optical scatter dynamic observed within the mitochondria-rich fluorescent regions. Thus the measured optical scatter dynamics are largely associated with mitochondria in the designated fluorescent regions above threshold. Low resolution and whole-cell detection of the decrease in orientedness (Figs. 3 and 5) was therefore also possible because of this null background contribution to the optical dynamic.

In addition, several findings support the hypothesis that mitochondrial alterations are the source of the measured optical scatter changes. Modulating the threshold which defines the fluorescent and nonfluorescent segments, results in modulating the optical scatter changes in the two compartments, suggesting that the optical scatter changes are spatially correlated with the fluorescence signal (Fig. 6). By considering the changes in orientedness at steady state timepoints well before and well after fragmentation, when the designated fluorescent and nonfluorescent segments should be accurate within 8%, we still find that orientedness is significantly changed only in the designated fluorescent regions and remains absent from the nonfluorescent ones (Fig. 7). Finally, the decrease in orientedness measured at the moment of fragmentation (between $T = 60$ and $T = 100$) in the designated fluorescent regions was not accompanied by an increase in orientedness in the designated nonfluorescent regions (Fig. 7). Thus, the measured decrease in orientedness could not be purely attributed to movement of oriented mitochondria from one segment to the other. Instead, mitochondrial fragmentation accompanied by movement of the mitochondria, would give rise to a decrease in orientedness in the fluorescent regions. At the same time, possible movement of the

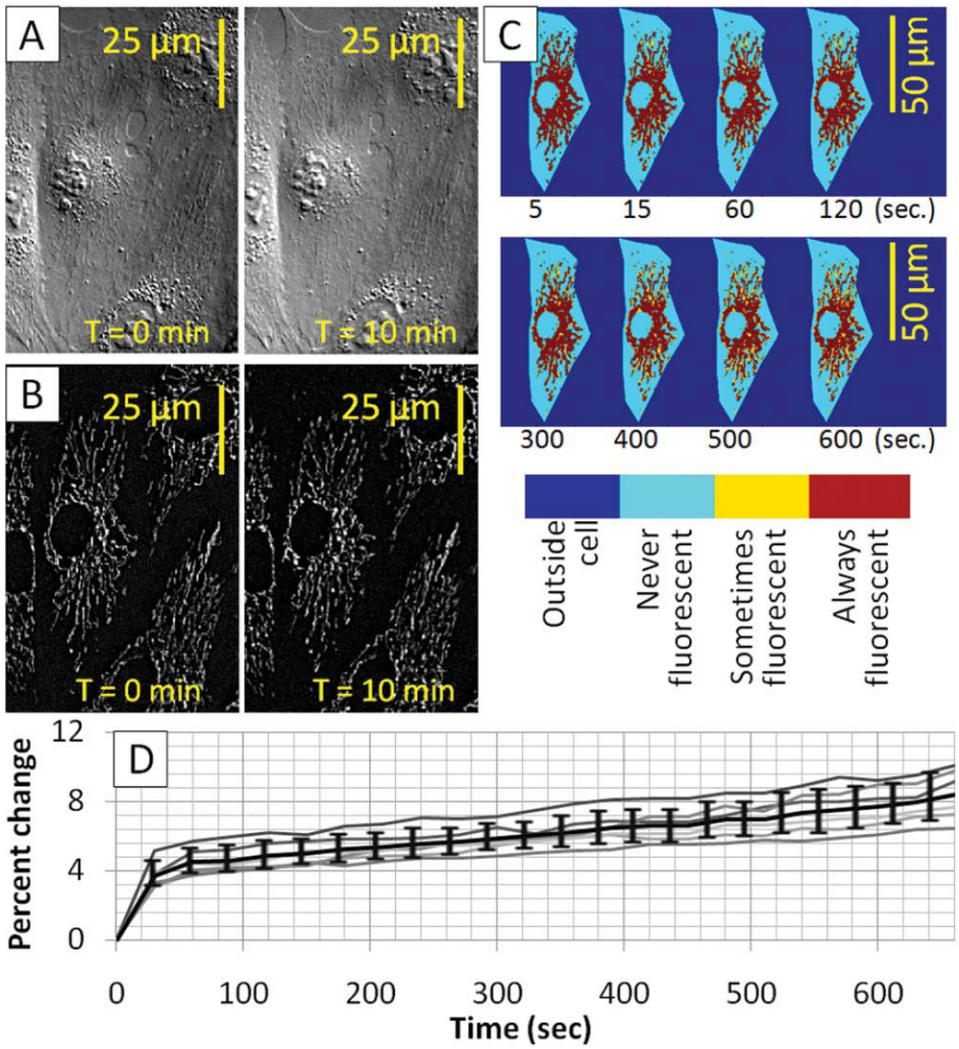


**Figure 8.** Effect of movement on accuracy of masks. DIC (**A**) and fluorescence (**B**) image of BAEC labeled with Mitotracker green under experimental conditions taken immediately after STS exposure ($T = 0$ minute) and 10 minutes later. (**C**) Color coded segments demonstrating how the segments within the ROI of a representative cell change over time. Each ROI is compared with the initial ROI at $T = 0$ in order to quantify movement over a 10-min time span. (**D**) Time trace plotting the fraction of pixels that changes between fluorescent and non-fluorescent regions over time. After an initial jump from zero to 5% by 1 minute, the error increases at a fairly constant rate of 0.4% per minute. Solid bold black trace represents the mean ± standard deviation of the gray traces of cells exposed to STS in this experiment.

fragmented mitochondria, which have low orientedness on the order of background (more blue in Figs. 3 and 5), to the non-fluorescent regions would keep the optical signal constant in these background regions. Still, current work focused on increasing light throughput and automation of the hardware, is under way to obtain faster optical scatter image acquisition, and thus minimize the effect of movement on the accuracy of multi-image registration, and allow better time resolution of subcellular dynamics.

As expected, the fragmentation of mitochondria (Fig. 4) and evidence of caspase 3 activation observed in the STS-treated BAEC (Fig. 9) reproduces previous evidence of mitochondrial fission in apoptotic cells treated with STS (35). In addition, alterations in light scattering concurrent with alteration in mitochondrial function during apoptosis have been reported (22,39,40). The present results extend these previous studies by showing that orientation-dependent changes in light scattering within the first 3 hours of apoptosis are spatially associated with mitochondria undergoing fragmentation, and can be directly quantified with an optical scatter imaging method based on Fourier filtering with Gabor-like filters.

In summary, our data provide strong evidence that mitochondrial fission can be monitored in situ within living cells through the use of light scattering signatures that depend on the degree of particle orientation. This method would have significant advantages in applications where sample labeling is cumbersome or where fluorescence labels may interfere with biological function. The ability to monitor the process at low image resolution at the whole cell level would also permit a higher cell analysis throughput. This method could be utilized

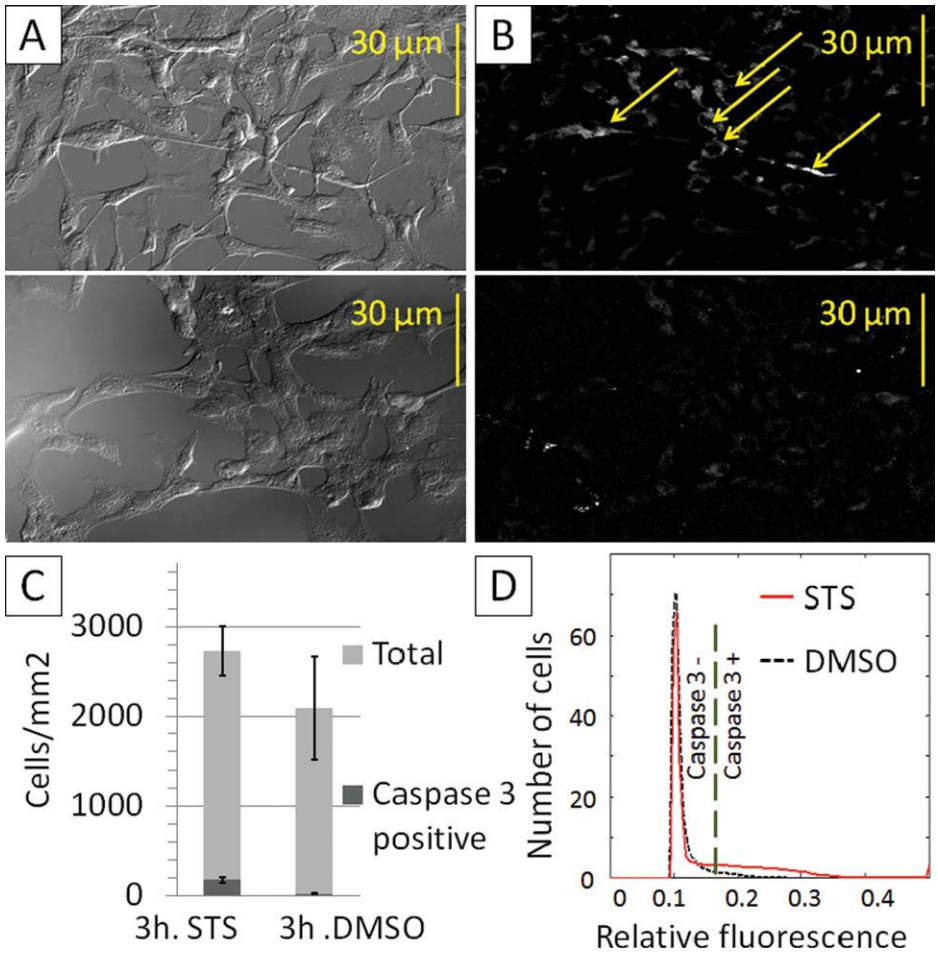


**Figure 9.** Immunofluorescence of cleaved caspase 3 in BAEC under experimental conditions. Representative DIC (**A**) and immunofluorescence (**B**) images of cells treated with STS (top) or DMSO (bottom) for 3 hours. Arrows point to cleaved caspase 3 positive cells in B, top panel. (**C**) Number of caspase 3 positive cells (dark gray) as a fraction of the total number of cells tested (light gray) for STS- and DMSO-treated cells. The ordinate cells/mm$^2$ is calculated by manually counting cells and normalizing to the area of the field of view measured with the aid of a stage micrometer. While small, the fraction of cleaved caspase 3 positive cells is significantly greater ($P < 0.01$) in the cells treated with STS than cells treated with DMSO. (**D**) Relative fluorescence intensity distributions for the STS- and DMSO-treated cells. Cells with intensity greater than 50% the background intensity (0.11) were taken as positive for caspase 3 activation. [Color figure can be viewed in the online issue, which is available at wileyonlinelibrary.com.]

to detect fragmentation of mitochondria during apoptosis as shown here. In this context, our results indicate that this technique may provide a tool that can be combined with molecular and biochemical methods to help facilitate elucidation of the structure-function relationship of mitochondria in apoptosis. In particular, the method can be used to investigate the presence of mitochondrial fission in response to activation (e.g. Bid activation) or knock out (e.g. Bax/Bak knock out) of Bcl-2 family proteins. Mitochondria undergo inner and outer membrane fission under the control of dynamin related proteins, which can interact with Bcl-2 family proteins during apoptosis. During apoptosis, truncated Bid (tBid) causes mitochondrial matrix vesicularization by disruption of OPA-1 oligomers, which control mitochondrial inner membrane fusion (41–43). tBid also affects bioenergetics, induces mitochondrial lipid peroxidation, and can activate Bax/Bak by interacting with cardiolipin (12,44). Interaction with mitochondrial membrane lipids and potential alteration of these lipids may be important in establishing mitochondrial structure. In addition, mitochondria fragment during apoptosis under the control of Drp-1 and Fis1 (35,45). Strong evidence suggests that Drp-1 is critical for mitochondrial outer-membrane permeabilization and release of cytochrome c. In particular during apoptosis Bax translocates to mitochondria and coalesces with Drp-1 and Mitofusin 2 (Mfn-2) at mitochondria fission sites (46), Bax is required to stabilize Drp1 localization on the mitochondria (47) and inhibition of Drp-1 inhibits Bax-mediated cytochrome c release and apoptosis (35,48). We had also found evidence of mitochondrial structural alterations in response to Bcl-$x_L$ overexpression (49). Thus, aided by the measurement method presented here, future studies of mitochondrial fission in response to Bid activation, Bax/Bak knock out, or Bcl-$x_L$ overexpression, could ultimately lead to important clues regarding the apoptotic function of mitochondrial dynamics. The approach presented here could also ultimately be translated to track mitochondrial fission in other systems.

## Acknowledgments

The authors thank Drs. Eileen White and Dimitris Metaxas for insightful discussions, and Kevin Bray from the White lab for assistance with the caspase assay.

## Literature Cited

1. Wallace DC. Mitochondrial diseases in man and mouse. Science 1999;283:1482–1488.
2. Detmer SA, Chan DC. Functions and dysfunctions of mitochondrial dynamics. Nat Rev Mol Cell Biol 2007;8:870–879.
3. Stoner CD, Sirak HD. Adenine nucleotide-induced contraction of the inner mitochondrial membrane. 1. General characterization. J Cell Biol 1973;56:51–64.
4. Stoner CD, Sirak HD. Adenine nucleotide-induced contraction of the inner mitochondrial membrane. 2. Effect of bongkrekic acid. J Cell Biol 1973;56:65–73.
5. Klingenberg M, Grebe K, Scherer B. Opposite effects of bongkrekic acid and atractyloside on the adenine nucleotides induced mitochondrial volume changes and on the efflux of adenine nucleotides. FEBS Lett 1971;16:253–256.
6. Halestrap AP. The regulation of the matrix volume of mammalian mitochondria in vivo and in vitro and its role in the control of mitochondrial metabolism. Biochim Biophys Acta 1989;973:355–382.
7. Eliseev RA, Salter JD, Gunter KK, Gunter TE. Bcl-2 and tbid proteins counter-regulate mitochondrial potassium transport. Biochim Biophys Acta 2003;1604:1–5.
8. Kowaltowski AJ, Cosso RG, Campos CB, Fiskum G. Effect of Bcl-2 overexpression on mitochondrial structure and function. J Biol Chem 2002;277:42802–42807.
9. Vander-Heiden MG, Chandel NS, Schumacker PT, Thompson CB. Bcl-xL prevents cell death following growth factor withdrawal by facilitating mitochondrial ATP/ADP exchange. Mol Cell 1999;3:159–167.
10. Belzacq A-S, Vieira HLA, Verrier F, Vandecasteele G, Cohen I, Prevost M-C, Larquet E, Pariselli F, Petit PX, Kahn A, Rizzuto R, Brenner C, Kroemer G. Bcl-2 and Bax Modulate Adenine Nucleotide Translocase Activity. Cancer Research 2003;63:541–546.
11. Doran E, Halestrap AP. Cytochrome c release from isolated rat liver mitochondria can occur independently of outer-membrane rupture: Possible role of contact sites. Biochem J 2000;348:343–350.
12. Gonzalvez F, Pariselli F, Jalmar O, Dupaigne P, Sureau F, Dellinger M, Hendrickson EA, Bernard S, Petit PX. Mechanistic issues of the interaction of the hairpin-forming domain of tBid with mitochondrial cardiolipin. PLoS One 2010;5:e9342.
13. Rossignol R, Gilkerson R, Aggeler R, Yamagata K, Remington SJ, Capaldi RA. Energy substrate modulates mitochondrial structure and oxidative capacity in cancer cells. Cancer Res 2004;64:985–993.
14. Alirol E, Martinou J. Mitochondria and cancer: Is there a morphological connection? Oncogene 2006;25:4706–4716.
15. Suen D-F, Norris KL, Youle RJ. Mitochondrial dynamics and apoptosis. Genes Dev 2008;22:1577–1590.
16. Hackenbrock CR. Ultrastructural bases for metabolically linked mechanical acivity in mitochondria I. J Cell Biol 1966;30:269–297.
17. Hunter DR, Haworth RA. The Ca2+-induced membrane transition in mitochondria. Arch Biochem Biophys 1979;195:453–459.
18. Bernardi P. Modulation of the mitochondrial cyclosporin A-sensitive permeability transition pore by the proton electrochemical gradient. J Biol Chem 1992;267:8834–8839.
19. Vander-Heiden MG, Chandel NS, Williamson EK, Schumacker PT, Thompson CB. Bcl-xL regulates the membrane potential and volume homeostasis of mitochondria. Cell 1997;91:627–637.
20. Zamzami N, Susin SA, Marchetti P, Hirsch T, Gomez-Monterrey I, Castedo M, Kroemer G. Mitochondrial control of nuclear apoptosis. J Exp Med 1996;183:1533–1544.
21. Petit PX, O'connor JE, Grunwald D, Brown SC. Analysis of the membrane potential of rat- and mouse-liver mitochondria by flow cytometry and possible applications. Eur J Biochem 1990;194:389–397.
22. Wilson JD, Giesselman BR, Mitra S, Foster TH. Lysosome-damage-induced scattering changes coincide with release of cytochrome c. Opt Lett 2007;32:2517–2519.
23. Gourley PL, Hendricks JK, McDonald AE, Copeland RG, Barrett KE, Gourley CR, Naviaux RK. Ultrafast nanolaser flow device for deteecting cancer in single cells. Biomed Microdevices 2005;7:331–339.
24. Quinlan PT, Thomas AP, Armston AE, Halestrap AP. Measurement of intramitochondrial volume in hepatocytes without cell disruption and its elevation by hormones and valinomycin. Biochem J 1983;214:395–404.
25. deGannes FMP, Belaud-Rotureau M-A, Voisin P, Leducq N, Belloc F, Canioni P, Diolez P. Flow cytometric analysis of mitochondrial activity in situ: Application to acetylceramide-induced mitochondrial swelling and apoptosis. Cytometry 1998;33:333–339.
26. Beauvoit B, Evans SM, Jenkins TW, Miller EE, Chance B. Correlation between the light scattering and the mitochondrial content of normal tissues and transplantable rodent tumors. Anal Biochem 1995;226:167–174.
27. Mannella CA. The relevance of mitochondrial membrane topology to mitochondrial function. Biochim Biophys Acta 2006;1762:140–147.
28. Karbowski M, Arnoult D, Chen H, Chan DC, Smith CL, Youle RY. Quantitation of mitochondrial dynamics by photolabeling of individual organelles shows that mitochondrial fusion is blocked during the Bax activation of apoptosis. J Cell Biol 2004;164:493–499.
29. Frezza C, Cipolat S, Scorrano L. Measuring mitochondrial shape changes and their consequences on mitochondrial involvement during apoptosis. Methods Mol Biol 2007;372:405–420.
30. Szabadkai G, Simoni A, Chami M, Wieckowski MR, Youle RJ, Rizutto R. Drp-1-dependent division of the mitochondrial network blocks intraorganellar $Ca^{2+}$ waves and protects against $Ca^{2+}$-mediated apoptosis. Mol Cell 2004;16:59–68.
31. Gerencser AA, Doczi J, Torocsik B, Bossy-Wetzel E, Adam-Vizi V. Mitochondrial swelling measurement in situ by optimized spatial filtering: Astrocyte-neuron differences. Biophys J 2008;95:2583–2598.
32. Pasternack RM, Qian Z, Zheng J-Y, Metaxas DN, Boustany NN. Highly sensitive size discrimination of submicron objects using optical fourier processing based on two-dimensional gabor filters. Opt Express 2009;17:12001–12012.
33. Pasternack RM, Qian Z, Zheng J, Metaxas DN, White E, Boustany NN. Measurement of subcellular texture by optical fourier filtering with a micromirror device. Opt Lett 2008;33:2209–2211.
34. Pasternack RM, Qian Z, Zheng J, Metaxas DN, White E, Boustany NN. Measurement of subcellular texture by optical fourier filtering with a micromirror device-erratum. Opt Lett 2009;34:1939.
35. Frank S, Gaume B, Bergmann-Leitner ES, Leitner WW, Robert EG, Catez F, Smith CL, Youle RJ. The role of dynamin-related protein 1, a mediator of mitochondrial fission, in apoptosis. Dev Cell 2001;1:515–525.
36. Boustany NN, Drezek R, Thakor NV. Calcium-induced alterations in mitochondrial morphology quantified in situ with optical scatter imaging. Biophys J 2002;83:1691–1700.
37. Wilson JD, Bigelow CE, Calkins DJ, Foster TH. Light scattering from intact cells reports oxidative-stress-induced mitochondrial swelling. Biophys J 2005;88:2929–2938.
38. Wilson JD, Cottrell WJ, Foster TH Index-of-refraction-dependent subcellular light scattering observed with organelle-specific dyes. J Biomed Opt 2007;12:014010.
39. Boustany NN, Tsai YC, Pfister B, Joiner WM, Oyler GA, Thakor NV. BCL-x(L)-dependent light scattering by apoptotic cells. Biophys J 2004;87:4163–4171.
40. Chalut KJ, Ostrander JH, Giacomelli MG, Wax A. Light scattering measurements of subcellular structure provide noninvasive early detection of chemotherapy-induced apoptosis. Cancer Res 2009;69:1199–1204.
41. Olichon A, Baricault L, Gas N, Guillou E, Valette A, Belenguer P, Lenaers G. Loss of OPA1 perturbates the mitochondrial inner membrane structure and integrity. Leading to cytochrome c release and apoptosis. J Biol Chem 2003;278:7743–7746.
42. Scorrano L, Ashiya M, Buttle K, Weiler S, Oakes SA, Mannella CA, Korsmeyer SJ. A distinct pathway remodels mitochondrial cristae and mobilizes cytochrome C during apoptosis. Dev Cell 2002;2:55–67.
43. Frezza C, Cipolat S, Brito OMd, Micaroni M, Beznoussenko GV, Rudka T, Bartoli D, Polishuck RS, Danial NN, deStrooper B, et al. OPA1 controls apoptotic cristae remodeling independently from mitochondrial fusion. Cell 2006;126:177–189.
44. Gonzalvez F, Pariselli F, Dupaigne P, Budihardjo I, Lutter M, Antonsson B, Diolez P, Manon S, Martinou JC, Goubern M, et al. tBid interaction with cardiolipin primarily orchestrates mitochondrial dysfunctions and subsequently activates Bax and Bak. Cell Death Differ 2005;12:614–626.
45. Alirol E, James D, Huber D, Marchetto A, Vergani L, Martinou J, Scorrano L. The mitochondrial fission protein hFis1 requires the endoplasmic reticulum gateway to induce apoptosis. Mol Biol Cell 2006;17:4593–4605.
46. Karbowski M, Lee Y-J, Gaume B, Jeong S-Y, Frank S, Nechushtan A, Santel A, Fuller M, Smith CL, Youle RJ. Spatial and temporal association of Bax with mitochondrial fission sites. Drp1, and Mfn2 during apoptosis. J Cell Biol 2002;159:931–938.
47. Wasiak S, Zunino R, McBride HM. Bax/Bak promote sumoylation of DRP1 and its stable association with mitochondria during apoptotic cell death. J Cell Biol 2007;177:439–450.
48. Cassidy-Stone A, Chipuk JE, Ingerman E, Song C, Yoo C, Kuwana T, Kurth MJ, Shaw JT, Hinshaw JE, Green DR, Nunnari J. Chemical inhibition of the mitochondrial division dynamin reveals its role in bax/bak-dependent mitochondrial outer membrane permeabilization. Dev Cell 2008;14:193–204.
49. Zheng J, Tsai Y, Kadimcherla P, Zhang R, Shi J, Oyler GA, Boustany NN. The C-terminal transmembrane domain of Bcl-xL mediates changes in mitochondrial morphology. Biophys J 2008;94:286–297.